ELSEVIER

www.elsevier.nl/locate/jorganchem

Journal of Organometallic Chemistry 601 (2000) 1–15

Journal of Organometallic Chemistry

Synthesis, characterization and X-ray structural determination of palladium(0)–olefin complexes containing pyridin-thioethers as ancillary ligands. Equilibria and rates of olefin and ligand exchange

Luciano Canovese [a,*], Fabiano Visentin [a], Gavino Chessa [a], Paolo Uguagliati [a], Alessandro Dolmella [b]

[a] *Dipartimento di Chimica, Universita' di Venezia, Venice, Italy*
[b] *Dipartimento di Scienze Farmaceutiche, Universita' di Padova, Padua, Italy*

Received 16 November 1999; accepted 5 January 2000

Abstract

The synthesis of Pd(0)–olefin complexes with pyridin-thioether ligands R′N–SR is reported. X-ray structure determinations of selected species are described. The dynamic behavior was studied by variable-temperature ^{1}H-NMR spectrometry. Equilibrium constants for olefin and chelate ligand exchange were determined by UV–vis spectrophotometry in chloroform at 25°C. The following metal–olefin stability order was observed: tetramethylethylenetetracarboxylate (tmetc) ≈ naphthoquinone (nq) < fumaronitrile (fn) ≈ maleic anhydride (ma) ≪ tetracyanoethylene (tcne). The ligand exchange equilibrium constants indicate that α-diimines and pyridin-thioethers affect the stability of the metal–bidentate ligand arrangement to a similar extent, as found in similar Pd(II) complexes. When the entering olefin is tmetc, the approach to equilibrium is slow so that both second-order rate constants k_2 and k_{-2} could be determined along with their activation parameters for the reversible reaction of [Pd(η^2-nq)(HN–S^{i}Pr)] with tmetc. The results indicate an associative mechanism to be operative in these olefin exchange processes.

Keywords: Palladium–olefin complexes; Thioethers; Equilibria; Olefin and ligand exchange

1. Introduction

We have been systematically studying the mechanism of nucleophilic attack at the allyl moiety in η^3-allyl palladium(II) cationic complexes containing bi- and terdentate (NN, NP, NS, NSN, SNS, PNN, NNN) ligands in the presence of activated olefins (ol) by tetraphenylborate ion or amines. The reactions involve allylphenylation or -amination with concomitant formation of palladium(0) olefin complexes of the type [Pd(ol)(polydentate ligand)] [1]. We have also studied the reverse of the amination reaction, i.e. the oxidative allyl transfer from allylammonium cations to [Pd(η^2-ol)(α-diimine)] [2]. It has become apparent that the stability of these zero-valent metal–olefin complexes, either as final products or reacting substrates, is of prime importance in the mechanistic pattern, being dictated by the nature of both the bidentate ligand and the olefin. In this context, we investigated equilibria and rates of olefin displacement in Pd(0) α-diimine complexes by activated, electron-poor olefins [3]. Equilibrium constants increased with increasing electron affinity of the entering olefin, whereas an associative pathway is operating for the slow, kinetically monitored reaction. These studies are among the few described so far concerning the stability and reactivity of zero-valent olefin complexes. Recently it has been shown that back donation of electron density from the metal to the olefin is the major factor affecting stability. Substitution of the olefin may occur via either associative or dissociative mechanisms, depending on the

* Corresponding author.
E-mail address: cano@unive.it (L. Canovese)

0022-328X/00/$ - see front matter
PII: S0022-328X(00)00014-0

steric requirements of the bidentate ligand [4]. Associative paths had also been proposed for olefin exchangein[Pt(C_2H_4)(PPh_3)$_2$][5]and[Pd(olefin)($PMePh_2$)$_2$] -[6] and for substitution of coordinated alkynes in [Pt(alkyne)(PPh_3)$_2$] complexes [7]. An interesting dynamic behavior is displayed by recently described palladium(0) complexes containing chelating diimines [4,8], P,N- [9], and P,S-donor ligands [10].

Several of these palladium–olefin substrates have interesting applications in some catalytic reactions either as precursors or as active species [8,11]. In view of these promising features and of the paucity of quantitative equilibrium and kinetic data available for these systems, we have investigated the thermodynamics and mechanism of substitution of the coordinated olefin by other, electron-poor olefins in complexes of N,S-donor chelating ligands R′N–SR of the type [Pd(ol)(R′N–SR)]

[Pd(η^2-ol)(R′N-SR)]

R′N-SR =

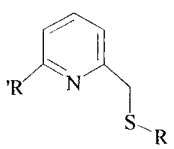

R' = H R = Me , Et , i-Pr , t-Bu , Ph
R' = Me R = Ph

ol = 1,4-naphthoquinone (nq)
fumaronitrile (fn)
maleic anhydride (ma)
tetramethylethylene tetracarboxylate (tmetc)
tetracyanoethylene (tcne)

Scheme 1.

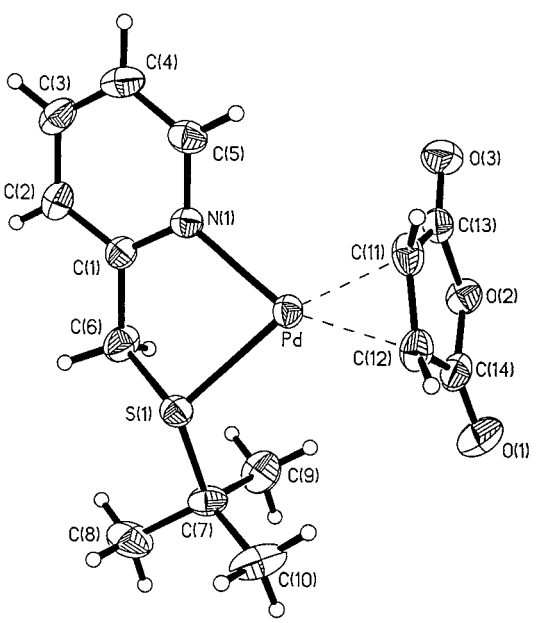

Fig. 1. Molecular structure of [Pd(η^2-ma)(HN–S′Bu)] in the crystal (50% probability displacement ellipsoids for non-H atoms and circles of arbitrary size for H atoms).

Table 1
Selected bond lengths (Å) and angles (°) for [Pd(η^2-ma)(HN–S′Bu)] and [Pd(η^2-tcne)(HN–SMe)]

[Pd(η^2-ma)(HN–S′Bu)]		[Pd(η^2-tcne)(HN–SMe)]	
Bond lengths			
Pd–S(1)	2.328(1)	Pd–S(1)	2.352(3)
Pd–N(1)	2.118(3)	Pd–N(1)	2.091(7)
Pd–C(11)	2.048(3)	S(1)–C(6)	1.817(9)
Pd–C(12)	2.063(3)	S(1)–C(7)	1.82(1)
S(1)–C(6)	1.799(4)	Pd–C(8)	2.085(9)
S(1)–C(7)	1.832(3)	Pd–C(9)	2.046(9)
C(11)–C(12)	1.413(5)	C(8)–C(9)	1.48(1)
O(2)–C(13)	1.397(4)		
O(2)–C(14)	1.400(4)		
Bond angles			
S(1)–Pd–N(1)	81.10(8)	S(1)–Pd–N(1)	83.3(2)
S(1)–Pd–C(11)	162.8(1)	S(1)–Pd–C(8)	160.5(2)
S(1)–Pd–C(12)	122.9(1)	S(1)–Pd–C(9)	118.4(3)
N(1)–Pd–C(11)	115.8(1)	N(1)–Pd–C(8)	116.2(3)
N(1)–Pd–C(12)	156.0(1)	N(1)–Pd–C(9)	157.9(4)
C(11)–Pd–C(12)	40.2(1)	C(8)–Pd–C(9)	42.1(4)
Pd–S(1)–C(6)	97.0(1)	Pd–S(1)–C(6)	95.3(3)
Pd–S(1)–C(7)	116.4(1)	Pd–S(1)–C(7)	102.5(4)
Pd–N(1)–C(1)	119.1(2)	C(6)–S(1)–C(7)	99.6(5)
C(12)–C(11)–C(13)	108.0(3)	C(10)–C(8)–C(11)	115.4(8)
C(11)–C(12)–C(14)	106.6(3)	C(12)–C(9)–C(13)	116.0(9)
C(13)–O(2)–C(14)	108.4(2)		

(Scheme 1) in chloroform. We hoped to relate the resulting equilibrium and kinetic data to steric and electronic properties of the chelating ligand, the coordinated olefin, and the entering one.

2. Results and discussion

2.1. X-ray diffraction studies

The molecular structure of complex [Pd(η^2-ma)(HN–S′Bu] has been confirmed by X-ray crystallography. The ORTEP diagram is shown in Fig. 1, while the selected bond distances and angles are listed in Table 1.

The bidentate HN–S′Bu ligand is coordinated to palladium and the coordination plane also comprises the double bond (C(11)=C(12)) of maleic anhydride. The palladium is situated on the least-squares plane defined by N,S,C(11) and C(12) atoms within a deviation of 0.026 Å from the plane. The coordinated anhydride is virtually planar (maximum deviation 0.04 Å by O(2)) and makes a dihedral angle of 78.5° with the mean coordination plane and 91.0° with the pyridine ring.

The five-membered Pd–N(1)–C(1)–C(6)–S(1) ring assumes an envelope conformation (C_s), with N(1), C(1) and S(1) below the mean plane by -0.14, -0.07 and -0.26 Å, respectively, while the Pd and C(6) atoms lie above this plane by $+0.19$ and $+0.28$ Å, respectively.

The C(11)–C(12) bond distance is significantly longer (0.11 Å) than in the free olefin, in line with other Pd(0)–ma complexes (Ref. [4] and references therein).

The Pd(0)–S distance (2.328(1) Å) is marginally shorter than the values of 2.365(1) [12] and 2.354(1) Å [10] found in the two other complexes containing the zero-valent metal, while it closely approaches the mean value (2.323 Å) encountered in 377 Pd(II)–S entries [13]. Analogously, the Pd(0)–N distance (2.118(3) Å) is slightly shorter than those observed for Pd(0)–N in the complexes reported so far (2.13 [14] and 2.16 Å [15]). The remaining bond distances are in the expected range and deserve no comment.

An ORTEP diagram of the molecular structure of [Pd(η^2-tcne)(HN–SMe)] is shown in Fig. 2, while the selected bond distances and angles are listed in Table 1.

This complex represents the sixth example of an X-ray structure containing the Pd(0)(tcne) fragment [12,16]. The C=C bond of η^2-coordinated tcne lies in the coordination plane and the palladium atom is situated on the least-squares plane defined by S(1), N(1), C(8) and C(9) within a deviation of 0.04 Å from the plane; the slight distortion from square planarity around the Pd center is reflected by the dihedral angle of 6.0° between Pd–S(1)–N(1) and Pd–C(8)–C(9) planes. Although the distances of Pd–C(8) and Pd–C(9) are slightly different from each other, they are close to those found in previous structures (in the range 2.054–2.111 Å) [12,16]. The coordinated tcne is non-planar and each cyano group is bent away from the Pd; the dihedral angle between two planes, one plane containing N(2), C(10), C(8), C(11) and N(3) and the other containing N(4), C(12), C(9), C(13) and N(5), is 127.7°. The C=C bond distance (1.49(1) Å) is longer than that of the uncoordinated one [17] by 0.15 Å, as a result of back donation from Pd to tcne. The five-membered chelate ring Pd–S(1)–C(6)–C(5)–N(1) adopts an envelope (C_s) conformation with S(1) above (by 0.69 Å) the Pd–N(1)–C(5)–C(6) plane. The Pd–N(1) distance (2.091(7) Å) agrees with the mean value (2.11 Å) observed for other 17 crystal structures [13] containing both sulfur and N (sp^2) donor atoms, while the Pd–S(1) distance (2.352(3) Å) is remarkably longer than the mean value (2.29 Å) in the same complexes.

In the unit cell the molecules are well separated, the shortest intermolecular interaction (2.59 Å) being between the N(2) atom and the hydrogen at C(1) of the molecule at $2-x$, $1-y$, $2-z$.

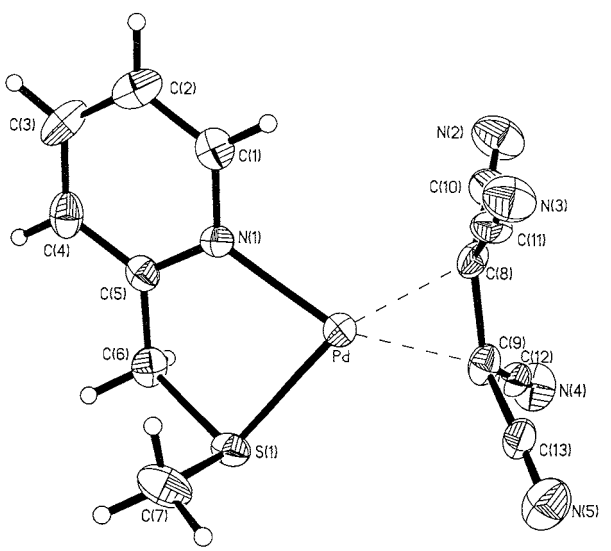

Fig. 2. Molecular structure of [Pd(η^2-tcne)(HN–SMe)] in the crystal (50% probability displacement ellipsoids for non-H atoms and circles of arbitrary size for H atoms).

2.2. NMR spectra and solution behavior

Selected ^{1}H-NMR data at low temperature for the η^2-olefin–Pd(0) complexes under study are listed in Tables 2 and 3, whereas ^{1}H- and ^{13}C{^{1}H}-NMR data at room temperature are reported in the Section 4.

It is convenient to distinguish the metal species on the basis of the type of olefin involved, i.e. symmetrically tetra-substituted (tcne, tmetc), type *E* (fn), and type *Z* (ma, nq). The corresponding complexes together with their diastereoisomers (when present) are shown in Scheme 2.

2.2.1. Symmetric olefins

The low-temperature ^{1}H-NMR spectra of complexes bearing these olefins display two characteristic features, namely an AB quartet ascribable to the CH_2S endocyclic protons and four singlets from the four different carboxylate methyl protons (in the case of ol = tmetc). These observations point to the presence of one single isomer, the enantiomeric forms due to the sulfur absolute configuration going undetected under our experimental conditions. Moreover, this evidence rules out a possible distinction between the two conformers arising from conformational flexibility of the five-membered N,S-chelate ring.

2.2.2. Type E olefins

In the case of ol = fn two diastereoisomers are possible, namely the *Re* and *Si* species referred to the olefin face coordinated to the metal center. Accordingly, the ^{1}H-NMR spectra at low temperature should show two AB systems due to CH_2S and two further AB systems due to olefin protons. The isomer relative population depends on the substituents R and R′ (Tables 2 and 3). However, the isomers *Re* and *Si* were not distinguishable.

2.2.3. Type Z olefins

As can again be seen in Scheme 2, in the case of complexes of *Z*-type olefins (ma, nq), two distinct diastereoisomers (together with their undetected enan-

Table 2
Selected ^{1}H-NMR data for [Pd(η^2-ol)(R′N–SR)] at low temperature[a]

Complex	CH_2–S	Olefin protons	R, R′ or H^6 (characteristic signals)	Stereoisomers ratio
[Pd(η^2-fn)(HN–SMe)]	A′ = 4.16 B′ = 4.04 J_{AB} = 16.7 A″ = 4.25 B″ = 4.08 J_{AB} = 16.5	A′ = 3.07 B′ = 3.02 J_{AB} = 9.5 A″ = 3.09 B″ = 2.98 J_{AB} = 9.4	CH_3, 2.22, 2.30	1.55:1
[Pd(η^2-fn)(HN–SEt)]	A′ = 4.24 B′ = 4.41 J_{AB} = 16.4 A″ = 4.15 B″ = 4.13 J_{AB} = 16.1	A′ = 3.10 B′ = 3.02 J_{AB} = 9.4 A″ = 3.09 B″ = 2.98 J_{AB} = 9.4	CH_2CH_3, 2.76, 1.28 (t), 2.62	1:1
Pd(η^2-fn)(HN–S^{i}Pr)]	A′ = 4.26 B′ = 4.16 J_{AB} = 16.7 A″ = 4.20 B″ = 4.16 J_{AB} = 16.7	A′ = 3.11 B′ = 2.99 J_{AB} = 9.3 A″ = 3.10 B″ = 3.02 J_{AB} = 9.4	$CH(CH_3)_2$, 3.05, 1.30	2:1
Pd(η^2-fn)(HN–S′Bu)]	Not resolved	A′ = 3.11 B′ = 2.98 J_{AB} = 9.5 A″ = 3.07 B″ = 3.02 J_{AB} = 9.2	$C(CH_3)_3$, 1.37, 1.35	2:1
[Pd(η^2-fn)(HN–SPh)]	A′ = 4.58 B′ = 4.44 J_{AB} = 16.5 A″ = 4.58 B″ = 4.41 J_{AB} = 16.5	A′ = 3.19 B′ = 3.16 J_{AB} = 9.4 A″ = 3.22 B″ = 3.14 J_{AB} = 9.4		1.25:1
[Pd(η^2-fn)(MeN–SPh)]	A′ = 4.58 B′ = 4.49 J_{AB} = 16.4 A″ = 4.54 B″ = 4.57 J_{AB} = 16.4	A′ = 3.19 B′ = 3.11 J_{AB} = 9.5 A″ = 3.17 B″ = 3.13 J_{AB} = 9.4	CH_3, 2.77, 2.81	2:1
[Pd(η^2-nq)(HN–SMe)]	A′ = 4.08 B′ = 3.96 J_{AB} = 16.4 A″ = 4.08 B″ = 3.94 J_{AB} = 16.4	Not resolved	CH_3, 1.89 (s), 2.32 (s)	1.6:1
[Pd(η^2-nq)(HN–SEt)]	A′ = 4.08 B′ = 3.92 J_{AB} = 16.5 A″ = 4.15 B″ = 4.02 J_{AB} = 16.5	A′ = 4.77 B′ = 4.71 J_{AB} = 6.9 A″ = 4.75 B″ = 4.69 J_{AB} = 6.9	CH_2CH_3, 2.33 (m) 0.7 (t), 2.80 (m) 1.3 (t)	3:1
[Pd(η^2-nq)(HN–S^{i}Pr)]	A′ = 4.16 B′ = 3.88 J_{AB} = 16.8 A″ = 4.16 B″ = 4.02 J_{AB} = 16.5	A′ = 4.78 B′ = 4.67 J_{AB} = 6.7 A″ = 4.78 B″ = 4.70 J_{AB} = 6.7	$CH(CH_3)_2$, 2.84 (bs) 0.93 (bd), 0.42 (bd), 3.24 (bs) 1.35 (bd), 1.30 (bd)	2.6:1
[Pd(η^2-nq)(HN–S′Bu)]	4.07 (bs) 4.04	A′ = 4.78 B′ = 4.66 J_{AB} = 6.9 A″ = 4.74 B″ = 4.66 J_{AB} = 6.9	$C(CH_3)_3$, 0.89, 1.43	1.7:1
[Pd(η^2-nq)(HN–SPh)]	Not resolved 4.33 (bs)	Not resolved 4.82 (bs)		2:1
[Pd(η^2-nq)(MeN–SPh)]	Not resolved 4.36 (bm)	A′ = 4.85 B′ = 4.70 J_{AB} = 7.1 A″ = 4.79 B″ = 4.65 J_{AB} = 7.2	CH_3, 2.76 (s), 2.58 (s)	1.9:1
[Pd(η^2-ma)(HN–SMe)]	[b]	[b]	CH_3H^6, 2.18, 8.67, 2.20, 8.80	1:0.8
[Pd(η^2-ma)(HN–SEt)]	[b]	[b]	$CH_2CH_3H^6$, 2.67 (bm) 1.17 (t) 8.67, 2.48 (bm) 1.25 (t) 8.76	2.25:1
[Pd(η^2-ma)(HN–S^{i}Pr)]	[b]	[b]	$CH(CH_3)_2H^6$, 2.91 (bm) 1.30 (bd) 8.6, 3.05 (bm) 1.14 (d) 8.3	2:1
[Pd(η^2-ma)(HN–S′Bu)]	[b]	[b]	$C(CH_3)_3$, 1.26, 1.36	1.8:1
[Pd(η^2-ma)(HN–SPh)]	4.47 (bs)	4.17 (bs)	H^6, 8.66, 8.77	1.4:1
[Pd(η^2-ma)(MeN–SPh)]	4.46 (bs) 4.52 (bs)	A′ = 4.20 B′ = 4.13 J_{AB} = 3.8 A″ = 4.20 B″ = 4.17 J_{AB} = 3.8	CH_3, 2.77 (s), 2.70 (s)	2:1

[a] A′, B′ = chemical shift (in ppm) more abundant diastereoisomer; A″, B″ = chemical shift (in ppm) less abundant diastereoisomer; J_{AB} = coupling constant (in Hz) AB systems.
[b] =CH_2–S and olefinic protons are almost isochronous and therefore not resolved.

tiomers) are possible, namely the *exo* and *endo* rotamers related to the mutual orientations of the group X within the olefin cycle with respect to the sulfur substituent R. Accordingly, two couples of AB systems are observed. Moreover, an unequal isomer distribution population (Tables 2 and 3) is observed in almost all cases. The relative position of groups X and R was not determined.

2.2.4. Fluxional behavior

On increasing the temperature, all complexes undergo two distinct fluxional processes, which can be interpreted by the following different mechanisms:

1. inversion of sulfur configuration;
2. olefin rotation (propeller-like);
3. Pd–olefin bond cleavage and recombination;
4. Pd–N or Pd–S bond cleavage followed by ancillary ligand rotation and rearrangement (olefin pseudo-rotation);
5. ancillary ligand intermolecular exchange.

Although these mechanisms are not equivalent, an appropriate combination of two of them is sufficient to explain the observed fluxionality of each species.

For symmetric olefin complexes (ol = tcne, tmetc), increasing the temperature causes the collapse of the CH_2S AB system accompanied by reduction to two of the initially four singlets belonging to methylcarboxylato protons. This phenomenon, which is independent of sample concentration, can only arise from inversion of the stereogenic coordinated sulfur (mechanism (1)) [10,18].

This behavior is similar to that observed for Pd(II) complexes, in which sulfur inversion is the only possible

mechanism [19]. One might argue that comparison among mechanisms involving palladium atoms in different oxidation states is not warranted. However, in our experience we noticed that sulfur inversion is always the first fluxional phenomenon occurring in any Pd complex bearing pyridin-thioether ligands and that the solution behavior of Pd(0) complexes containing electron-withdrawing olefins is similar in many respects to that of Pd(II) complexes [1g].

On increasing the temperature further, the collapse of the surviving singlets is observed. Any of the proposed mechanisms combined with mechanism (1) is consistent with the increase in molecular symmetry.

However, we propose the view that the second observed fluxional phenomenon involves propeller-like rotation of the olefin, or olefin pseudo-rotation (mechanism (4)), which in this case cannot a priori be ruled out. In the case of the more sterically demanding substituents (R = ^{i}Pr, ^{t}Bu), we cannot exclude a concomitant dissociation mechanism due to steric interaction between the bulky R groups and the hindered olefin tmetc [9,11,20].

As for the complexes with *E*-type olefins such as fn, which turns out to be more strongly bound and less sterically hindered than tmetc (see below), their fluxional behavior is somewhat more complicated and less diagnostic than the previously described cases. Sulfur inversion brings about the interchange between the diastereoisomers (Scheme 2) with concomitant reduction to two of the four AB systems (two arising from CH_2–S endocyclic protons and two from olefinic protons). Propeller-like olefin rotation is probably the next process taking place on increasing the temperature. Indeed, such rotation will not alter the chirality of palladium (persistence of the *Si* or *Re* face for coordinated olefins). Thus, one would expect to observe the persistence of an AB system for CH_2–S protons while the olefin proton AB system disappears (combination of mechanisms (1) and (2)). This is clearly borne out by [Pd(η^2-fn)(MeN–SPh)] and [Pd(η^2-fn)(HN–SEt)], in which the CH_2–S proton AB system barely persists at $T \approx 273$ and 296 K, respectively, while the olefin protons give rise to a singlet ($\delta = 3.16$ and 3.09 ppm, respectively). This finding rules out any of the dissociative mechanisms (3) or (5) (Fig. 3).

As for complexes bearing *Z*-type olefins, again two rotamers (*exo* and *endo*) along with their enantiomers are expected (Scheme 2). Sulfur inversion causes the disappearance of two of the four AB systems. The olefin rotation ensuing from a further increase in temperature (which will convert *exo* into *endo* forms and vice versa) coupled to the persisting sulfur inversion will explain the symmetry of ^{1}H-NMR spectra at higher temperatures.

Table 3
Selected ^{1}H-NMR signals at low temperature for complexes [Pd(η^2-tcne)(R′N–SR)] and [Pd(η^2-tmetc)(R′N–SR)]

Complex	CH_2–S	COOCH_3
[Pd(η^2-tcne)(HN–SMe)]	A = 4.38 B = 4.13	
	J_{AB} = 16.8	
[Pd(η^2-tcne)(HN–SEt)]	A = 4.35 B = 4.19	
	J_{AB} = 17.1	
[Pd(η^2-tcne)(HN–S^{i}Pr)]	A = 4.34 B = 4.22	
	J_{AB} = 16.9	
[Pd(η^2-tcne)(HN–S′Bu)]	A = 4.34 B = 4.27	
	J_{AB} = 17.1	
[Pd(η^2-tcne)(HN–SPh)]	A = 4.69 B = 4.53	
	J_{AB} = 16.8	
[Pd(η^2-tcne)(MeN–SPh)]	A = 4.70 B = 4.64	
	J_{AB} = 16.8	
[Pd(η^2-tmetc)(HN–SMe)]	A = 4.26 B = 4.04	3.62
	J_{AB} = 16.8	
		3.60
		3.58
		3.57
[Pd(η^2-tmetc)(HN–SEt)]	A = 4.28 B = 4.11	3.61
	J_{AB} = 16.8	
		3.59
		3.58
		3.57
[Pd(η^2-tmetc)(HN–S^{i}Pr)]	A = 4.29 B = 4.15	3.56 (2 Me)
	J_{AB} = 16.6	
		3.60 (2 Me)
[Pd(η^2-tmetc)(MeN–S′Bu)]	A = 4.23 B = 4.13	3.58 (3 Me)
	J_{AB} = 15.2	
		3.54 (1Me)
[Pd(η^2-tmetc)(HN–SPh)]	A = 4.59 B = 4.45	3.62 (2 Me)
	J_{AB} = 16.5	
		3.56 (1 Me)
		3.33 (1 Me)
[Pd(η^2-tmetc)(MeN–SPh)]	A = 4.57 B = 4.51	3.62
	J_{AB} = 16.5	
		3.59
		3.58
		3.28

3. Olefin substitution rate and equilibria

3.1. Olefin substitution rate constants

The rate of approach to equilibrium (1)

$$\underset{\mathbf{A}}{[Pd(\eta^2\text{-nq})(R'N\text{–}SR)]} + \underset{\mathbf{B}}{tmetc} \rightleftharpoons \underset{\mathbf{C}}{[Pd(\eta^2\text{-tmetc})(R'N\text{–}SR)]} + \underset{\mathbf{D}}{nq} \quad (1)$$

in chloroform at 25°C was determined by UV–vis spectrophotometric techniques. Spectral changes with time were monitored in the range 540–300 nm in the presence of a constant excess of tmetc over the metal substrate ($[Pd]_0 = 1 \times 10^{-4}$ mol dm^{-3}), in order to provide pseudo-first order conditions and to minimize the contribution of the reverse reaction (k_{-2}) to the overall spectral changes. Under these conditions the absorbance D_t obeys the mono-exponential rate law $D_t = D_\infty + (D_0 - D_\infty)\exp(-k_{obs}t)$, where D_0, D_∞ and

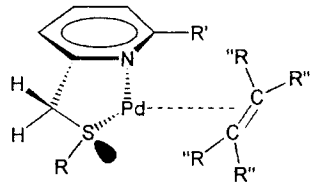

R' = H ; R = Me , Et , *i*-Pr , *t*-Bu , Ph ; R" = COOMe , CN

R' = Me ; R = Ph ; R" = COOMe , CN

Si *Re*

R' = H ; R = Me , Et , *i*-Pr , *t*-Bu , Ph ; R" = CN

R' = Me ; R = Ph ; R" = CN

endo *exo*

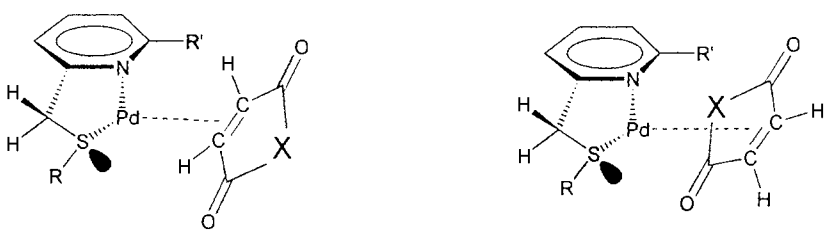

R' = H ; R = Me , Et , *i*-Pr , *t*-Bu , Ph ; X = O , C_6H_4

R' = Me ; R = Ph ; X = O , C_6H_4

Scheme 2.

k_{obs} are the initial, final absorbance, and the observed rate constant, respectively. The k_{obs} values, determined by non-linear regression where D_0, D_∞ and k_{obs} are the parameters to be optimized, fit the expression

$$k_{obs} = k_2[\text{tmetc}] \quad (2)$$

The resulting values for k_2 are listed in Table 4.

The k_{-2} parameters were determined by carrying out kinetic runs under second-order conditions in both directions, with tmetc concentrations comparable to those of the metal complex ([Pd] = 1×10^{-4} mol dm^{-3}, [tmetc] = 1×10^{-4}–6×10^{-4} mol dm^{-3}). Absorbance data were fitted to time according to the rate model for second-order reversible reactions [3]:

$$-\mathrm{d}[\mathbf{A}]/\mathrm{d}t = k_2[\mathbf{A}]([\mathbf{B}]_0 - [\mathbf{A}]_0 + [\mathbf{A}]) - k_{-2}([\mathbf{A}]_0 - [\mathbf{A}])^2 \quad (3)$$

where $[\mathbf{A}]_0$ and $[\mathbf{B}]_0$ are initial concentrations and $[\mathbf{C}] = [\mathbf{D}] = [\mathbf{A}]_0 - [\mathbf{A}] = [\mathbf{B}]_0 - [\mathbf{B}]$. The absorbance was given by

$$D_t = \varepsilon_A[\mathbf{A}] + \varepsilon_C[\mathbf{C}] + \varepsilon_D[\mathbf{D}] \quad (4)$$

($\varepsilon_B \cong 0$ in the wavelength range examined), where the species concentrations are derived from integration of Eq. (3) [3] and the relevant mass-balance equations. Non-linear regression of D_t values was carried out using k_{-2} as the parameter to be optimized, with the k_2 term being held fixed at the value determined earlier under pseudo-first-order conditions. This allowed re-

moval of the strong correlation between k_2 and k_{-2}, which is peculiar to the model being fitted and would unfavorably affect the convergence rate of the fitting procedure. The k_{-2} values are listed in Table 4, in which the equilibrium constants K_E for Eq. (1), as the ratios k_2/k_{-2}, are also reported. In the case of complex [Pd(η^2-nq)(HN–S^{t}Bu)], which reacts very slowly with tmetc, only pseudo-first-order conditions for the forward reaction could be employed to achieve conversion to an appropriate extent in a reasonable time period compatible with slow decomposition phenomena. On the other hand, the reverse reaction of [Pd(η^2-tmetc)(HN–S^{t}Bu)] with excess free nq could not be monitored owing to unfavorable spectral features (viz. the overly high extinction coefficients of nq).

From Table 4 it appears that both k_2 and k_{-2} are affected by the steric hindrance of the R substituent at the thioetheric sulfur. An LFER of $\log k_2$ versus the front strain steric parameter S of R [21] is shown in Fig. 4.

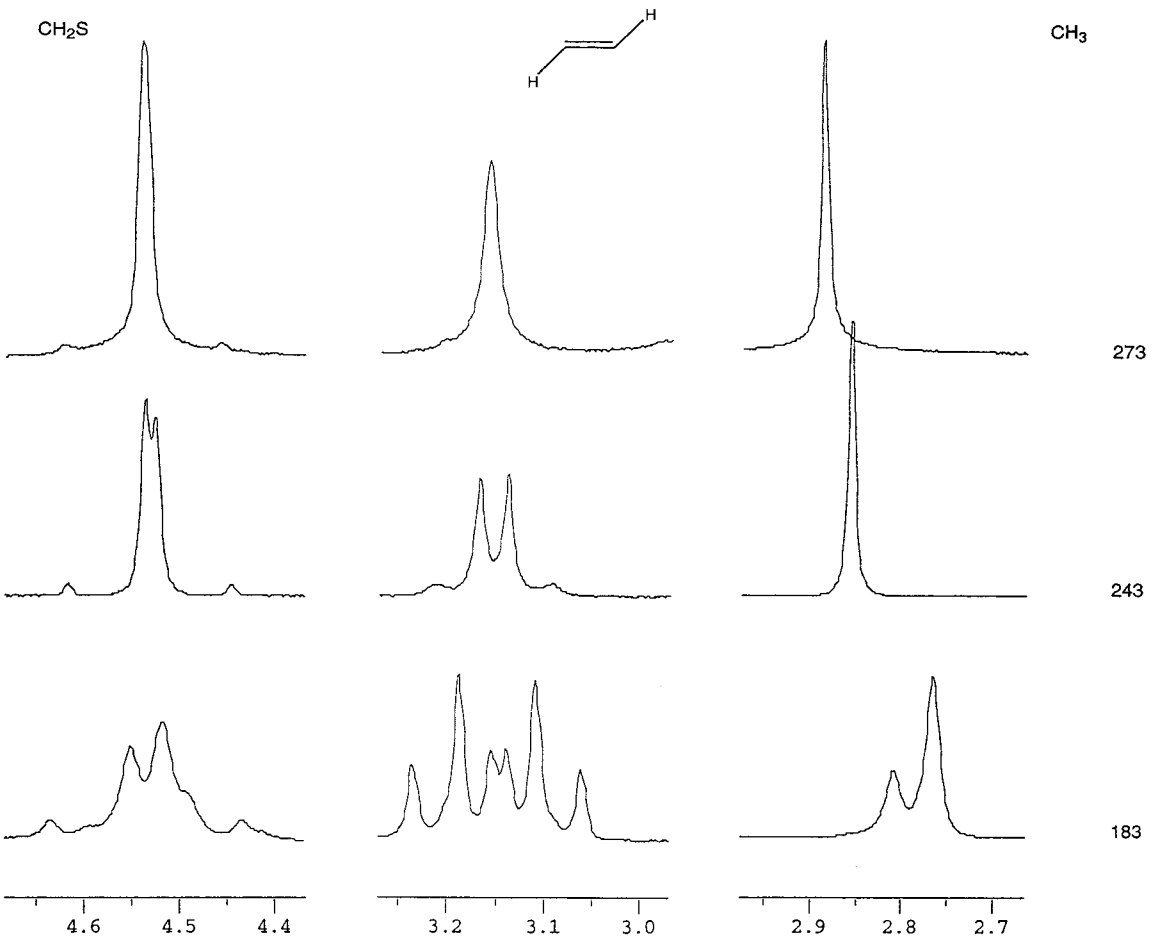

Fig. 3. Selected ^{1}H-NMR spectra of [Pd(η^2-fn)(MeN–SPh)] in CD_2Cl_2 at different temperatures.

Table 4
Second-order rate constants for the forward and reverse reactions (k_2 and k_{-2}) and calculated equilibrium constants (K_E) for equilibrium reaction (1); equilibrium constants for olefin substitution reactions (reaction (5)) in $CHCl_3$ at 25°C

Complex	tmetc		K_E		
	k_2 (mol^{-1} dm^3 s^{-1})	k_{-2} (mol^{-1} dm^3 s^{-1})	tmetc (k_2/k_{-2})	fn	ma
[Pd(η^2-nq)(HN–SMe)]	64 ± 5	42 ± 17	1.5 ± 0.6	17 ± 1	18 ± 1
[Pd(η^2-nq)(HN–SEt)]	14.6 ± 0.5	7.5 ± 2.5	1.9 ± 0.6	12 ± 2	16 ± 2
[Pd(η^2-nq)(HN–S^{i}Pr)]	1.40 ± 0.06	2.1 ± 0.3	0.7 ± 0.1	6.7 ± 0.4	9 ± 1
[Pd(η^2-nq)(HN–S^{t}Bu)]	$(2.95 \pm 0.04)10^{-2}$	0.05 ± 0.03 [a]	0.6 ± 0.4 [a]	5.5 ± 0.2	6.9 ± 0.4
[Pd(η^2-nq)(HN–SPh)]	6.7 ± 0.2	14.6 ± 5	0.5 ± 0.7	8.4 ± 0.9	7.2 ± 0.3
[Pd(η^2-nq)(MeN–SPh)]	1.7 ± 0.1	2.2 ± 0.5	0.8 ± 0.2	16 ± 1	49 ± 4

[a] Calculated values (see text).

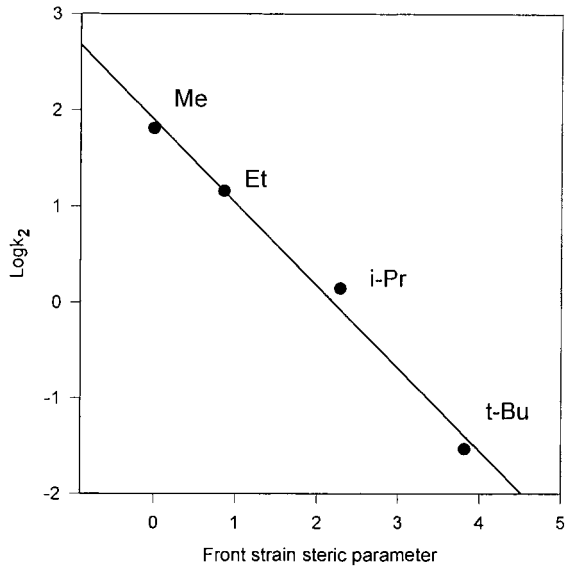

Fig. 4. Plot of $\log k_2$ for the reaction of [Pd(η^2-nq)(HN–SR)] with tmetc vs. the front strain steric parameter S of substituent R.

On the other hand, changes in electronic effects on changing R are hardly likely to affect the activation process of olefin attack. This suggests that these processes of olefin substitution are essentially associative in nature. This is confirmed by the comparatively low activation enthalpy ($\Delta H^{\#} = 10.2 \pm 0.5$ kcal mol^{-1}) and fairly negative activation entropy ($\Delta S^{\#} = -24 \pm 2$ cal mol^{-1} K^{-1}) for the k_2 step relating to [Pd(η^2-nq)(HN–S^{i}Pr)] reacting with tmetc, as deduced from the temperature dependence of k_2 in the range 15–45°C analyzed with the Eyring equation. Similar activation parameters had been determined for olefin substitution in analogous [Pd(η^2-ol)(N–N′)] complexes reacting with tmetc (ol = nq, dmf; N–N′ = 2-NC_5H_4CH=NC_6H_4OMe-4) [3]. The low activation enthalpy and the highly negative activation entropy found for these reactions are in agreement with an associative mechanism in which both the entering and the leaving olefins are present in an 18-electron transition state of an activation process involving considerable freezing of degrees of freedom. Associative mechanisms involving a bis-olefin-activated state have been proposed for olefin or alkyne substitution or exchange in Pd and Pt zero-valent complexes [4–7]. Similar adverse effects of the steric requirements of R are observed for the reverse reaction path k_{-2}, although the lack of the value for R = ^{t}Bu limits the LFER to only three experimental points (R = Me, Et, ^{i}Pr).

A gross estimate of k_{-2} (R = ^{t}Bu) can be attempted by extrapolation of the straight line to the appropriate front strain parameter. The ensuing value is fairly close to that determined from equilibrium and kinetic data, as described below. Activation parameters for k_{-2} are very close to those for the forward step k_2, indicating a common associative mechanism for both paths, as expected. Steric hindrance to approach by the entering olefin is also exerted by the R′ substituent in position 2 of the pyridine ring (cf. k_2 and k_{-2} for R′N–SR, R′ = H, Me, R = Ph). This is compounded by some rate-depressing effect due to the donor ability of the Me group, which is expected to disfavor formation of the 18-electron bis-olefin-activated complex through increased basicity of the pyridine nitrogen. However, the contributions of these phenomena to the overall rate effect are hard to untangle. The K_E values for equilibrium in Eq. (1), obtained as the rate constant ratios k_2/k_{-2} (Table 4), are close to unity in all cases, as expected on the basis of the similar stability of the two Pd(0)–olefin complexes involved as far as this is governed by the electron-withdrawing ability of the olefin substituents. This feature seems to be hardly affected by the bidentate ligand since it also occurs with other complexes [3].

3.2. Olefin substitution equilibrium constants

Equilibrium constants for the reactions

$$[\mathrm{Pd}(\eta^2\text{-nq})_{\mathbf{1}}(\mathrm{R'N–SR})] + \mathrm{ol} \rightleftharpoons [\mathrm{Pd}(\eta^2\text{-ol})_{\mathbf{2}}(\mathrm{R'N–SR})] + \mathrm{nq} \quad (\mathrm{ol} = \mathrm{ma},\ \mathrm{fn}) \tag{5}$$

in $CHCl_3$ were determined by recording spectral changes in the range 300–600 nm of mixtures obtained by adding appropriate microaliquots of solutions of ol to a solution of **1** ([Pd]$_0$ ca. 1×10^{-4} mol dm^{-3}) in the thermostatted cell compartment of the spectrophotometer. The equilibria were rapidly established. Absorbance data were analyzed at 400 nm where the change in absorbance was the largest and the olefins ol and nq do not absorb appreciably.

Under these conditions abstract factor analysis [22] of the observed spectral changes indicated that at most two independently absorbing species were present, i.e. complexes **1** and **2**. The absorbance data D_λ were fitted by non-linear least-squares according to the model

$$K_E = [\mathbf{2}][\mathrm{nq}]/[\mathbf{1}][\mathrm{ol}]$$

$$[\mathrm{Pd}]_{tot} = [\mathbf{1}] + [\mathbf{2}]$$

$$[\mathrm{nq}] + [\mathrm{ol}] = [\mathrm{nq}]_0 + [\mathrm{ol}]_0$$

$$[\mathrm{nq}] = [\mathrm{nq}]_0 + [\mathbf{2}]$$

$$D_\lambda = \varepsilon_1[\mathbf{1}] + \varepsilon_2[\mathbf{2}]$$

The parameters to be optimized were K_E and ε_2. The latter was either held constant at the experimentally accessible value (from the spectrum of complex **2** independently prepared) or allowed to float during the iterative process. In the latter case the final, optimized value turned out to coincide with that determined directly (Fig. 5).

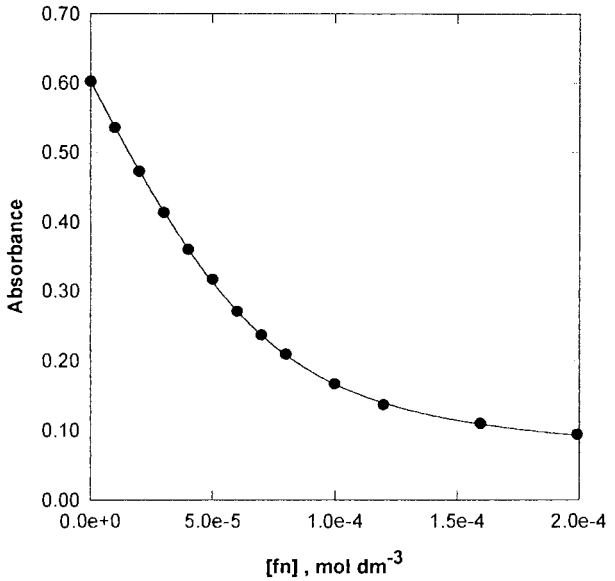

Fig. 5. Fit of absorbance at 400 nm to [fn] for the reaction of [Pd(η^2-nq)(HN–S^{t}Pr)] with fn in $CHCl_3$ at 25°C.

The K_E values are also listed in Table 4.

As can be seen, the K_E values cover a narrow range, spanning at most one order of magnitude. In particular, the complexes with ma and fn are in general more stable ($K_E \gg 1$) than those of nq, thanks to the higher electron-withdrawing ability of the former olefins, ma being more efficient than fn in this respect. This behavior is in agreement with our previous findings about olefin exchange in [Pd(η^2-ol)(α-diimine)] complexes [3]. Changing the bidentate ligand from 2-NC_5H_4CH=NC_6H_4OMe-4 to the present pyridin-thioether ligands does not significantly affect the olefin exchange equilibrium constants, other things being equal. However a moderate adverse effect of the steric requirement of the sulfur alkyl substituent (R) can be detected for both ma and fn. This might indicate that some sort of leveling in the electron-withdrawing properties of the olefins involved takes place, due to steric hindrance that overcomes the increasing electron-releasing ability of R, which would be expected to enhance the stability of complexes containing the more electronegative olefins ma and fn [23].

The discriminating effect of the higher electron affinity [23] of ma and fn is clearly borne out when an electron-donor methyl substituent is introduced into position 2 of the pyridine ring in complexes with R = Ph (cf. Table 4). As for the displacement of nq by tmetc, steric and electronic effects are much harder to discuss owing to the narrow range covered and the large uncertainties arising from the kinetic origin of the K_E values.

3.3. Ligand exchange equilibrium constants

We devised a procedure to evaluate the olefin exchange equilibrium constant K_E for the reaction of [Pd(η^2-nq)(HN–S^{t}Bu)] with tmetc by the use of the following equilibrium network:

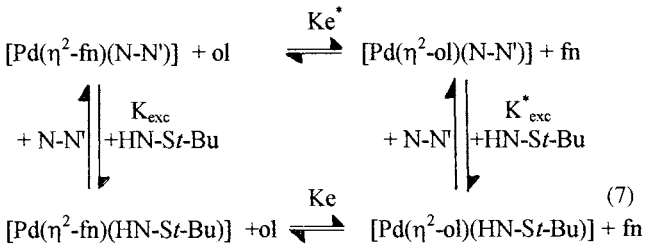

(7)

(ol = tmetc , nq , ma)
(N-N' = 2-NC_5H_4CH=NC_6H_4OMe-4)

$$Ke^{*}K^{*}_{exc} = K_{exc}Ke \quad (8)$$

The appropriate K_E^* data were available from our previous work [3]. The ligand exchange equilibrium constants K_{exc} and K^*_{exc} (ol = tmetc) were determined by spectrophotometric titration involving addition of appropriate aliquots of $CHCl_3$ solutions of HN–S^{t}Bu to solutions of [Pd(η^2-fn)(N–N′)] or [Pd(η^2-tmetc)(N–N′)] ([Pd]$_0$ ca. 1×10^{-4} mol dm^{-3}). Absorbance data were analyzed according to a procedure analogous to that described above for the olefin substitution equilibria. The resulting K_{exc} and K^*_{exc} are 7 ± 1 and 2.5 ± 0.6(ol = tmetc). Since K_E^* (ol = tmetc) $= 0.28 \pm 0.17$ [3], relationship (8) yields $K_E = 0.10 \pm 0.07$.

This calculated value combined with the measured one ($K_E = 5.5 \pm 0.2$ Table 4; referring to the exchange reaction between [Pd(η^2-nq)(HN–S^{t}Bu)] and fn) yields the equilibrium constant for the non-directly accessible case, in which tmetc exchanges with nq when the pyridin-thioether ligand is HN–S–^{t}Bu (see Table 4).

In the case of ol = nq, ma, the K_E^* and K_E values were available from our previous work [3] and the present work, respectively (Table 4), so that Eqs. (7) and (8) were used to evaluate K^*_{exc}. The ensuing K^*_{exc} values are 5 ± 2 (ol = nq) and 5 ± 3 (ol = ma). These data indicate that the relative bonding abilities of HN–S^{t}Bu and 2-NC_5H_4CH=NC_6H_4OMe-4 ligands for these Pd(0) moieties are almost independent of olefin and confined in a very narrow interval, thereby reflecting the observed feature in the case of Pd(II) η^3-allyl complexes [1g,h].

The K_E value for ol = tmetc, as deduced from network (7) and reported in Table 4 as a calculated value (0.6 ± 0.4), allows us to evaluate the k_{-2} rate constant for the reaction of [Pd(η^2-tmetc)(HN–S^{t}Bu)] with nq from the rate constant k_2 for the reverse reaction (Table 4). The resulting value (0.05 ± 0.04 mol^{-1} dm^3 s^{-1}) is in good agreement with that grossly estimated from the LFER based on front strain steric parameters S (see above) [21].

4. Experimental

The pyridin-thioether ligands (R′N–SR) [1g] and the complex $Pd_2(DBA)_3{\cdot}CHCl_3$ [24] were prepared according to published procedures. All other chemicals were commercial grade and were purified or dried, where required, by standard methods [25].

4.1. Preparation of complexes [Pd(η²-ol)(R′N–SR)]

The synthesis, the complete characterization and elemental analysis of the complexes [Pd(η²-fn)(R′N–SR)] (R′ = H, R = Et, ᵗBu, Ph; R′ = Me, R = Ph) are reported elsewhere [1f,g]. However a standard preparative procedure is reported here for [Pd(η²-nq)(HN–SMe)]. Because of the straightforward method of preparation, all complexes under study can be completely characterized by their multinuclear NMR spectral data and by their peculiar IR features. Therefore we only report herein the elemental analysis of some representative complexes.

4.1.1. [Pd(η²-nq)(HN–SMe)]

To a solution of HN–SMe (0.06 g, 0.44 mmol) in anhydrous acetone (10 cm^3) $Pd_2DBA_3{\cdot}CHCl_3$ (0.21 g, 0.2 mmol) and naphthoquinone (0.07 g, 0.44 mmol) were added under nitrogen. The reaction mixture was stirred for 1 h and the initial dark suspension turned to orange–red. Addition of activated charcoal and filtration on Celite removed metallic palladium yielding an orange–red solution. Reduction to small volume (3–4 cm^3) and addition of diethyl ether (15 cm^3) gave an orange precipitate, which was filtered off and washed with diethyl ether in excess to remove the free DBA. The crystals were dried under vacuum and stored under inert atmosphere (orange microcrystals, 0.12 g, yield 75%). Found: C, 50.72; H, 3.55; N, 3.38. $C_{17}H_{15}NO_2SPd$ requires: C, 50.57; H, 3.74; N, 3.47%. IR (in KBr) (cm^{-1}): $\nu_{C=O}$, 1626, 1610 (d)): $\nu_{C=N}$, 1581 (s), 1556 (s). ^{1}H-NMR (in $CDCl_3$, r.t.), δ (ppm): CH_2–S, 4.00 (2H, s); S–CH_3, 2.18 (3H, s); *H*C=C*H*, 4.94 (2H, s, H^g); H^3, H^5, 7.38 (2H, m); H^4, 7.77 (td, $J = 7.7$, 1.7 Hz); H^6, 8.51 (d, $J = 5.7$ Hz); H^e, 8.04 (2H, m); H^f, 7.48 (2H, m). ^{13}C{^{1}H}-NMR (in $CDCl_3$, r.t.), δ (ppm): *C*H$_2$–S, 43.6; S–*C*H$_3$, 20.0; C^2, 157.1; C^3, 124.7; C^4, 137.9; C^5, 123.2; C^6, 150.4; H*C*=*C*H, 65.0 (2C, C^g, broad); C^e, 124.2 (2C); C^f, 131.0 (2C).

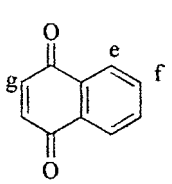

4.1.2. [Pd(η²-nq)(HN–SEt)]

The title complex was prepared in the same way as [Pd(η²-nq)(HN–SMe)] (red–brown microcrystals, yield 84%). IR (in KBr) (cm^{-1}): $\nu_{C=O}$, 1625 (s); $\nu_{C=N}$, 1587 (s). ^{1}H-NMR (in $CDCl_3$, r.t.), δ (ppm): CH_2–S, 4.02 (2H, s); S–CH_2, 2.57 (2H, q, $J = 7.4$ Hz); SCH$_2$–CH_3, 1.06 (3H, t, $J = 7.4$ Hz); *H*C=C*H*, 4.93 (2H, s, H^g); H^3, H^5, 7.35 (2H, m); H^4, 7.75 (td, $J = 7.7$, 1.7 Hz); H^6, 8.47 (d, $J = 5.3$ Hz); H^f, 7.48 (2H, m); H^e, 8.04 (2H, m). ^{13}C{^{1}H}-NMR (in $CDCl_3$, r.t.), δ (ppm): *C*H$_2$–S, 41.6; S–*C*H$_2$, 31.27; SCH$_2$–C*H*$_3$, 13.98; C^2, 158.0; C^3, 125.1; C^4, 138.2; C^5, 123.1; C^6, 150.2; H*C*=*C*H, 64.6 (C^g); C^e, 124.3 (2C); C^f, 131.2 (2C).

4.1.3. [Pd(η²-nq)(HN–SⁱPr)]

The title complex was prepared in the same way as [Pd(η²-nq)(HN–SMe)] (orange microcrystals, yield 86%). IR (in KBr) (cm^{-1}): $\nu_{C=O}$, 1632, 1616; $\nu_{C=N}$, 1585. ^{1}H-NMR (in $CDCl_3$, r.t.), δ (ppm): CH_2–S, 4.03 (2H, bs); S–C*H*, 2.96 (1H, sept, $J = 6.7$ Hz); CH(CH_3)$_2$, 1.09 (6H, bs); *H*C=C*H*, 4.91 (2H, bs, H^g); H^3, H^5, 7.4 (2H, m); H^4, 7.75 (td, $J = 7.7$, 1.7 Hz); H^6, 8.46 (d, $J = 5.0$ Hz); H^e, 8.04 (2H, m); H^f, 7.48 (2H, m). ^{13}C{^{1}H}-NMR (in $CDCl_3$, r.t.), δ (ppm): *C*H$_2$–S, 41.4; S–*C*H, 40.5; CH(*C*H$_3$)$_2$, 22.5; C^2, 158.5; C^3, 125.1; C^4, 138.14; C^5, 124.2; C^6, 149.8; H*C*=*C*H, 61.84 (C^g); C^e, 124.2; (2C); C^f, 131 (2C).

4.1.4. [Pd(η²-nq)(HN–SᵗBu)]

The title complex was prepared in the same way as [Pd(η²-nq)(HN–SMe)] (orange microcrystals, yield 83%). IR (in KBr) (cm^{-1}): $\nu_{C=O}$, 1628 (s), 1587 (s); $\nu_{C=N}$ obscured. ^{1}H-NMR (in $CDCl_3$, r.t.), δ (ppm): CH_2–S, 4.03 (2H, s); C(CH_3)$_3$, 1.22 (9H, s); *H*C=C*H*, 4.87, 4.89 (2H, H^g, bs); H^3, 7.4 (1H, d, $J = 7.6$ Hz); H^4, 7.75 (td, $J = 7.6$, 1.2 Hz); H^5, 7.5 (partially obscured by H^3); H^6, 8.5 (d, $J = 5.1$ Hz); H^e, 8.03 (2H, m); H^f, 7.47 (2H, m). ^{13}C{^{1}H}-NMR (in $CDCl_3$, r.t.), δ (ppm): *C*H$_2$–S, 38.7; *C*(CH$_3$)$_3$, 48.9; C(*C*H$_3$)$_3$, 30.1 (3C); C^2, 158.7; C^3, 124.2; C^4, 138.1; C^5, 122.6; C^6, 149.7; HC=CH, 60.7, 66.1 (2C, C^g); C^e, 124.8, 125.3 (2C); C^f, 131.0, 131.3 (2C).

4.1.5. [Pd(η²-nq)(HN–SPh)]

The title complex was prepared in the same way as [Pd(η²-nq)(HN–SMe)] (dark orange microcrystals, yield 84%). IR (in KBr) (cm^{-1}): $\nu_{C=O}$, 1620, 1626; $\nu_{C=N}$, 1586 (s) ^{1}H-NMR (in $CDCl_3$, r.t.), δ (ppm): CH_2–S, 4.33 (2H, s); *H*C=C*H*, 4.96 (2H, H^g, s); H^3, H^5, H^b, H^c, H^d, 7.25 (7H, m); H^4, 7.73 (td, $J = 7.7$, 1.7 Hz); H^6, 8.51 (d, $J = 5.3$ Hz); H^e, 8.00 (2H, m); H^f, 7.47 (2H, m). ^{13}C{^{1}H}-NMR (in $CDCl_3$, r.t.), δ (ppm): *C*H$_2$–S, 46.25; C^a (obscured); C^b, 129.0; C^c, 131.1; C^d, 128.6; C^2, 156.9; C^3, 124.1; C^4, 137.9; C^5, 122.8; C^6, 148.8; H*C*=*C*H (obscured); C^e, 125.0 (2C); C^f, 131.4 (2C).

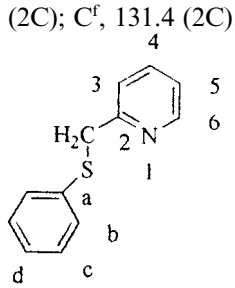

4.1.6. [Pd(η²-nq)(MeN–SPh)]

The title complex was prepared in the same way as [Pd(η²-nq)(HN–SMe)] (red–brown microcrystals, yield 79%). IR (in KBr) (cm^{-1}): $\nu_{C=O}$, 1639, 1630; $\nu_{C=N}$, 1589, ^{1}H-NMR (in $CDCl_3$, r.t.), δ (ppm): CH_2–S, 4.32 (2H, s); pyr–CH_3, 2.81 (3H, s); *H*C=C*H*, 4.9 (2H, s H^g); H^4, 7.56 (t, $J = 8.0$ Hz); H^5, 7.07 (d, $J = 8.0$ Hz); H^3, H^b, H^c, H^d, 7.27 (6H, m); H^e, 7.98 (2H, m); H^f, 7.50 (2H, m). ^{13}C{^{1}H}-NMR (in $CDCl_3$, r.t.), δ (ppm): *C*H$_2$–S, 47.0; pyr–*C*H$_3$, 28.2; C^b, 129.2; C^c, 131.5; C^d, 128.9; C^2, 159.0; C^3, 123.7; C^4, 137.9; C^5, 120.4; C^6, 156.5; C^e, 125.7, 125.3 (2C); C^f, 131.3, 132.2 (2C); *C*=O, 185.4.

4.1.7. [Pd(η²-ma)(HN–SMe)]

The title complex was prepared in the same way as [Pd(η²-nq)(HN–SMe)] (yellow microcrystals, yield 80%). Found: C, 38.81; H, 3.05; N, 4.02. $C_{11}H_{11}NO_3SPd$ requires: C, 38.44; H, 3.23; N, 4.08%. IR (in KBr) (cm^{-1}): $\nu_{C=O}$, 1795 (s), 1722 (s); $\nu_{C=N}$, 1599, ^{1}H-NMR (in $CDCl_3$, r.t.), δ (ppm): CH_2S, 4.11 (2H, s); S–CH_3, 2.34 (3H, s); *H*C=C*H*, 4.17 (2H, s); H^4, 7.84 (td, $J = 7.7$, 1.7 Hz); H^3, 7.5 (d, $J = 7.7$ Hz); H^5, 7.35 (dd, $J = 7.7$, 5.2 Hz); H^6, 8.85 (d, $J = 5.2$ Hz). ^{13}C{^{1}H}-NMR (in $CDCl_3$, r.t.), δ (ppm): *C*H$_2$–S, 44.0; S–*C*H$_3$, 19.8; H*C*=*C*H, 46.0; C^2, 156.9; C^3, 124.0; C^4, 138.2; C^5, 123.7; C^6, 153.0; *C*=O, 71.5.

4.1.8. [Pd(η²-ma)(HN–SEt)]

The title complex was prepared in the same way as [Pd(η²-nq)(HN–SMe)] (yellow microcrystals, yield 75%) (decomposes slowly in the solid and in chlorinated solvents). IR (in KBr) (cm^{-1}): $\nu_{C=O}$, 1790, 1724; $\nu_{C=N}$, 1598. ^{1}H-NMR (in $CDCl_3$, r.t.), δ (ppm): CH_2–S, 4.13 (2H, s); S–CH_2, 2.73 (2H, q, $J = 7.4$ Hz); SCH$_2$–CH_3, 1.34 (3H, t, $J = 7.4$ Hz); *H*C=C*H*, 4.20 (2H, bs); H^4, 7.83 (td, $J = 7.7$, 1.6 Hz); H^3, 7.48 (d, $J = 7.7$ Hz); H^5, 7.35 (td, $J = 7.7$, 4.9 Hz); H^6, 8.85 (d, $J = 4.9$ Hz). ^{13}C{^{1}H}-NMR (in $CDCl_3$, r.t.), δ (ppm): *C*H$_2$–S, 42.3; S–*C*H$_2$, 31.3; SCH$_2$–*C*H$_3$, 14.25; H*C*=*C*H, 45.78; C^2, 157.6; C^3, 124.2; C^4, 138.41; C^5, 123.5; C^6, 153.2 *C*.

4.1.9. [Pd(η²-ma)(HN–S^{i}Pr)]

The title complex was prepared in the same way as [Pd(η²-nq)(HN–SMe)] (yellow microcrystals, yield 90%, decomposes slowly in chlorinated solvents). IR (in KBr) (cm^{-1}): $\nu_{C=O}$, 1790 (s), 1722 (s); $\nu_{C=N}$, 1600. ^{1}H-NMR (in $CDCl_3$, r.t.), δ (ppm): CH_2–S, 4.15 (2H, s); S–C*H*, 3.08 (1H, sept, $J = 6.7$ Hz); CH(CH_3)$_2$, 1.36 (6H, d, $J = 6.7$ Hz); *H*C=C*H*, 4.15 (2H, s); H^4, 7.83 (td, $J = 7.7$, 1.6 Hz); H^3, 7.48 (d, $J = 7.7$ Hz); H^5, 7.33 (dd, $J = 7.7$, 4.7); H^6, 8.83 (d, $J = 4.7$ Hz). ^{13}C{^{1}H}-NMR (in $CDCl_3$, r.t.), δ (ppm): *C*H$_2$–S, 41.1; S–*C*H, 40.9; CH(*C*H$_3$)$_2$, 23.0; H*C*=*C*H, 45.8 (b); C^2, 158.1; C^3, 124.1; C^4, 138.4; C^5, 123.2; C^6, 153.1; *C*=O, 171.0 (b).

4.1.10. [Pd(η²-ma)(HN–S^{t}Bu)]

The title complex was prepared in the same way as [Pd(η²-nq)(HN–SMe)] (yellow microcrystals, yield 86%). IR (in KBr) (cm^{-1}): $\nu_{C=O}$, 1790 (s), 1724 (s); $\nu_{C=N}$, 1601. ^{1}H-NMR (in $CDCl_3$, r.t.), δ (ppm): CH_2–S, 4.17 (2H, s); S–C(CH_3)$_3$, 1.42 (9H, s,) HC=CH, 4.14 (2H, s); H^3, 7.49 (d, $J = 7.8$ Hz); H^4, 7.82 (td, $J = 7.8$, 1.7 Hz); H^5 (dd, $J = 7.8$, 5.2 Hz); H^6, 8.82 (d, $J = 5.2$). ^{13}C{^{1}H}-NMR (in $CDCl_3$, r.t.), δ (ppm): *C*H$_2$–S, 39.1; S–*C*(CH$_3$)$_3$, 48.9; C(*C*H$_3$)$_3$, 30.5; H*C*=*C*H, 45.5; C^2, 158.6; C^3, 124.1; C^4, 138.4; C^5, 123.0; C^6, 153.0.

4.1.11. [Pd(η²-ma)(HN–SPh)]

The title complex was prepared in the same way as [Pd(η²-nq)(HN–SMe)]. (yellow microcrystals, yield 82%) IR (in KBr) (cm^{-1}): $\nu_{C=O}$, 1791, 1724; $\nu_{C=N}$, 1597. ^{1}H-NMR (in $CDCl_3$, r.t.), δ (ppm): CH_2–S, 4.45 (2H, s); *H*C=C*H*, 4.26 (2H, s); H^3, H^5, H^c, H^d, 7.37 (5H, m); H^b, 7.57 (2H, m); H^4, 7.80 (td, $J = 7.7$, 1.7 Hz); H^6, 8.86 (d, $J = 5.3$ Hz). ^{13}C{^{1}H}-NMR (in $CDCl_3$, r.t.), δ (ppm): *C*H$_2$–S, 47.2; H*C*=*C*H, 47.0; C^b, 129.7; C^c, 131.8; C^d, 129.4; C^3, 129.4; C^4, 138.5; C^5, 123.4; C^6, 153.1.

4.1.12. [Pd(η²-ma)(MeN–SPh)]

The title complex was prepared in the same way as [Pd(η²-nq)(HN–SMe)] (yellow microcrystals, yield 86%). IR (in KBr) (cm^{-1}): $\nu_{C=O}$, 1794 (s), 1726 (s); $\nu_{C=N}$, 1601. ^{1}H-NMR (in $CDCl_3$, r.t.), δ (ppm): CH_2–S, 4.49 (2H, s); pyr–CH_3, 2.88 (3H, s); *H*C=C*H*, 4.23 (2H, s); H^3, H^b, H^c, H^d, 7.43 (6H, m); H^4, 7.66 (t, $J = 8.0$ Hz); H^5, 7.21 (d, $J = 8.0$ Hz). ^{13}C{^{1}H}-NMR (in $CDCl_3$, r.t.), δ (ppm): *C*H$_2$–S, 46.7; pyr–*C*H$_3$, 29.1; H*C*=*C*H, 45.6; C^b, 129.3; C^c, 131.3; C^d, 129.0; C^2, 161.1; C^3, 123.6; C^4, 138.0; C^5, 120.3; C^6, 156.4.

4.1.13. [Pd(η²-fn)(HN–SMe)]

The title complex was prepared in the same way as [Pd(η²-nq)(HN–SMe)] (white microcrystals, yield 75%, decomposes slowly in chlorinated solvent). Found: C, 41.03; H, 3.38; N, 12.81. $C_{11}H_{11}N_3SPd$ requires: C, 40.81; H, 3.43; N, 12.98%. IR (in KBr) (cm^{-1}): $\nu_{C\equiv N}$, 2196 (s); $\nu_{C=N}$, 1598 (s). ^{1}H-NMR (in $CDCl_3$, r.t.), δ (ppm): CH_2–S, 4.16 (2H, s); S–CH_3, 2.39 (3H, s); *H*C=C*H*, 3.10 (2H, s); H^3, 7.51 (d, $J = 7.7$ Hz); H^4, 7.86 (td, $J = 7.7$, 1.7 Hz); H^5, 7.38 (dd, $J = 7.7$, 5.1 Hz); H^6, 8.95 (d, $J = 5.1$ Hz). ^{13}C{^{1}H}-NMR (in $CDCl_3$, r.t.), δ (ppm): S–*C*H$_2$, 44.3; S–*C*H$_3$, 20.0; H*C*=*C*H, 22.4; *C*≡N, 122.3; C^2, 157.1; C^3, 124.2; C^4, 138.4; C^5, 123.9; C^6, 153.4.

4.1.14. [Pd(η²-fn)(HN–SEt)]

The title complex [1f] was prepared in the same way as [Pd(η²-nq)(HN–SMe)] (white microcrystals, yield

63%, decomposes slowly in chlorinated solvents). IR (in KBr) (cm^{-1}): $\nu_{C\equiv N}$, 2197 (s): $\nu_{C=N}$, 1597. ^{1}H-NMR (in $CDCl_3$, r.t.), δ (ppm): CH_2–S, 4.16, 4.21(2H, $J = 16.2$ Hz, AB syst.); S–CH_2, 2.88 (2H, q, $J = 7.4$ Hz); CH_2CH_3, 1.40 (t, $J = 7.4$ Hz); HC=C*H*, 3.10 (2H, bs); H^3, 7.5 (d, $J = 7.7$ Hz); H^4, 7.85 (td, $J = 7.7$, 1.5 Hz); H^5, 7.35 (dd, $J = 7.7$, 5.1 Hz); H^6, 8.9 (d, $J = 5.1$ Hz). ^{13}C{^{1}H}-NMR (in $CDCl_3$, r.t.), δ (ppm): *C*H_2–S, 42.14; S–*C*H_2, 31.1; CH_2–*C*H_3, 14.0; HC=*C*H, 22.5; *C*≡N, 122.41; C^2, 157.6; C^3, 124.14; C^4, 138.4; C^5, 123.61; C^6, 153.4.

4.1.15. [Pd(η^2-fn)(HN–S^{i}Pr)]

The title complex was prepared in the same way as [Pd(η^2-nq)(HN–SMe)] (yellow microcrystals yield 80%, decomposes slowly in chlorinated solvents). IR (in KBr) (cm^{-1}): $\nu_{C\equiv N}$, 2197 (s); $\nu_{C=N}$, 1599. ^{1}H-NMR (in $CDCl_3$, r.t.), δ (ppm): CH_2–S, 4.20 (2H, s); S–C*H*, 3.12 (1H, sept, $J = 6.7$ Hz); $CH(CH_3)_2$, 1.43 (6H, d, $J = 6.7$ Hz); HC=C*H*, 3.12 (2H, s); H^3, 7.5 (d, $J = 7.7$ Hz); H^4, 7.85 (td, $J = 7.7$, 1.6 Hz); H^5, 7.35 (dd, $J = 7.7$, 5.3 Hz); H^6, 8.92 (d, $J = 5.3$ Hz). ^{13}C{^{1}H}-NMR (in $CDCl_3$, r.t.), δ (ppm): *C*H_2–S, 41.0; S–*C*H, 40.6; $CH(CH_3)_2$, 22.9; HC=*C*H, 22.4; *C*≡N, 122.5; C^2, 158.0; C^3, 124.1; C^4, 138.4; C^5, 123.3; C^6, 153.3.

4.1.16. [Pd(η^2-fn)(HN–S^{t}Bu)]

The title complex [1g] was prepared in the same way as [Pd(η^2-nq)(HN–SMe)] (white microcrystals, yield 87%, decomposes slowly in the solid). IR (in KBr) (cm^{-1}): $\nu_{C\equiv N}$, 2199 (s); $\nu_{C=N}$, 1597. ^{1}H-NMR (in $CDCl_3$, r.t.), δ (ppm): CH_2–S, 4.2 (2H, s); S–C(CH_3)$_3$, 1.5 (9H, s); HC=C*H*, 3.1 (2H, bs); H^3, 7.51 (d, $J = 7.7$ Hz); H^4, 7.84 ($J = 7.7$, 1.6 Hz); H^5, 7.34 (dd, $J = 7.7$, 5.1 Hz); H^6, 8.85 (d, $J = 5.1$ Hz). ^{13}C{^{1}H}-NMR (in $CDCl_3$, r.t.), δ (ppm): *C*H_2–S, 39.0; S–*C*(CH_3)$_3$, 48.6; C(*C*H_3)$_3$, 30.4; HC=*C*H, 22.3; *C*≡N, 122.6; C^2, 158.0; C^3, 124.0; C^4, 138.4; C^5, 123.2; C^6, 153.1.

4.1.17. [Pd(η^2-fn)(HN–SPh)]

The title complex [1f] was prepared in the same way as [Pd(η^2-nq)(HN–SMe)] (white microcrystals, yield 78%). IR (in KBr) (cm^{-1}): $\nu_{C\equiv N}$, 2199 (s); $\nu_{C=N}$, 1601. ^{1}H-NMR (in $CDCl_3$, r.t.), δ (ppm): CH_2–S, 4.5 (2H, s); HC=C*H*, 3.2 (2H, s); H^3, H^5, H^b, H^c, H^d, 7.4 (7H, m); H^4, 7.88 (td, $J = 7.7$, 1.6 Hz); H^6, 8.95 (d, $J = 5.0$ Hz). ^{13}C{^{1}H}-NMR (in $CDCl_3$, r.t.), (ppm): *C*H_2–S, 47.1; HC=*C*H, 23.3; *C*≡N, 122.0; C^b, 129.4; C^c, 132.0; C^d, 129.3; C^2, 156.7; C^3, 124.0; C^4, 138.3; C^5, 123.3; C^6, 152.9.

4.1.18. [Pd(η^2-fn)(MeN–SPh)]

The title complex [1g] was prepared in the same way as [Pd(η^2-nq)(HN–SMe)] (yellowish microcrystals, yield 82%, decomposes slowly in chlorinated solvents). IR (in KBr) (cm^{-1}): $\nu_{C\equiv N}$, 2200 (s); $\nu_{C=N}$, 1602. ^{1}H-NMR (in $CDCl_3$, r.t.), δ (ppm): CH_2–S, 4.51 (2H, s); pyr–CH_3, 2.93 (3H, s); HC=C*H*, 3.18 (2H, s); H^4, 7.67 (t, $J = 7.7$ Hz); H^3, H^5, H^b, H^c, H^d, 7.40 (m). ^{13}C{^{1}H}-NMR (in $CDCl_3$, r.t.), (ppm): *C*H_2–S, 46.9; pyr–*C*H_3, 29.4; HC=*C*H, 23.0; *C*≡N, 122.3; ca. 131.4; C^b, 129.6; C^c, 131.6; C^d, 129.3; C^2, 161.1; C^3, 123.9; C^4, 138.3; C^5, 120.7; C^6, 156.7.

4.1.19. [Pd(η^2-tmetc)(HN–SMe)]

The title complex was prepared in the same way as [Pd(η^2-nq)(HN–SMe)] (yellow microcrystals, yield 94%). Found: C, 40.60; H, 4.11; N, 2.69. $C_{17}H_{21}NO_8SPd$ requires: C, 40.37; H, 4.18; N, 2.77%. IR (in KBr) (cm^{-1}): $\nu_{C=O}$, 1724, 1691; $\nu_{C=N}$, 1601. ^{1}H-NMR (in $CDCl_3$, r.t.), δ (ppm): CH_2–S, 4.14 (2H, s); S–CH_3, 2.48 (3H, s); O–CH_3, 3.7 (12H, s); H^3, 7.42 (d, $J = 7.7$ Hz); H^4, 7.78 (td, $J = 7.7$, 1.7 Hz); H^5, 7.32 (dd, $J = 7.7$, 5.4 Hz); H^6, 9.13 (d, $J = 5.4$ Hz). ^{13}C{^{1}H}-NMR (in $CDCl_3$, r.t.), δ (ppm): *C*H_2–S, 43.9; S–*C*H_3, 20.5; O–*C*H_3, 52; *C*=O, 169.9; C^2, 157.3; C^3, 123.7; C^4, 137.7; C^5, 123.1; C^6, 153.7.

4.1.20. [Pd(η^2-tmetc)(HN–SEt)]

The title complex was prepared in the same way as [Pd(η^2-nq)(HN–SMe)] (yellow microcrystals, yield 91%). IR (in KBr) (cm^{-1}): $\nu_{C=O}$, 1740, 1724, 1701, 1668; $\nu_{C=N}$, 1598. ^{1}H-NMR (in $CDCl_3$, r.t.), δ (ppm): CH_2–S, 4.16 (2H, s); S–CH_2, 2.86 (2H, q, $J = 7.4$ Hz); CH_2–CH_3, 1.34 (3H, t, $J = 7.4$ Hz); O–CH_3, 3.72 (12 H, s); H^3, 7.41 (d, $J = 7.7$ Hz); H^4, 7.77 (td, $J = 7.7$, 1.7 Hz); H^5, 7.31 (dd, $J = 7.7$, 5.2 Hz); H_6, 9.14 (d, $J = 5.2$ Hz). ^{13}C{^{1}H}-NMR (in $CDCl_3$, r.t.), δ (ppm): *C*H_2–S, 41.9; S–*C*H_2, 31.5; CH_2–*C*H_3, 14.14; O–*C*H_3, 52.21; C^2, 158.0; C^3, 123.86; C^4, 137.92; C^5, 122.9; C^6, 153.8; *C*=O, 169.9, 169.4

4.1.21. [Pd(η^2-tmetc)(HN–S^{i}Pr)]

The title complex was prepared in the same way as [Pd(η^2-nq)(HN–SMe)] (yellow microcrystals, yield 87%). IR (in KBr) (cm^{-1}): $\nu_{C=O}$, 1738, 1722, 1701, 1674; $\nu_{C=N}$, 1598. ^{1}H-NMR (in $CDCl_3$, r.t.), δ (ppm): CH_2–S, 4.16 (2H, s); S–C*H*, 3.23 (1H, sept, $J = 6.7$ Hz); $CH(CH_3)_2$, 1.37 (6H, d $J = 6.7$ Hz); O–CH_3, 3.70 (6H, s), O–CH_3, 3.71 (6H, s); H^3, 7.41 (d, $J = 7.7$ Hz); H^4, 7.76 (td, $J = 7.7$, 1.7 Hz); H^5, 7.32 (dd, $J = 7.7$, 5.3 Hz); H^6, 9.16 (d, $J = 5.3$ Hz). ^{13}C{^{1}H}-NMR (in $CDCl_3$, r.t.), δ (ppm): *C*H_2–S, 40.4; S–*C*H, 40.61; $CH(CH_3)_2$, 22.7; O–*C*H_3, 52.1; C^2, 158.33; C^3, 123.74; C^4, 137.9; C^5, 122.7; C^6, 153.8; *C*=O, 169.4, 169.9.

4.1.22. [Pd(η^2-tmetc)(HN–S^{t}Bu)]

The title complex was prepared in the same way as [Pd(η^2-nq)(HN–SMe)] (yellow microcrystals, yield 90%). IR (in KBr) (cm^{-1}): $\nu_{C=O}$, 1710, 1691; $\nu_{C=N}$, 1595 (s). ^{1}H-NMR (in $CDCl_3$, r.t.), δ (ppm): CH_2–S, 4.16 (2H, s); C(CH_3)$_3$, 1.43 (9H, s); O–CH_3, 3.70 (6H, s),

O–CH_3, 3.71 (6H, s); H^3, 7.42 (d, $J = 7.7$ Hz); H^4, 7.76 (td, $J = 7.7$, 1.7 Hz); H^5, 7.28 (dd, $J = 7.7$, 5.3 Hz); H^6, 9.15 (d, $J = 5.3$ Hz). $^{13}C\{^1H\}$-NMR (in $CDCl_3$, r.t.), δ (ppm): CH_2–S, 38.9; S–*C*, 48.0; C(CH_3)$_3$, 29.8; O–CH_3, 52.1; C^2, 158.6; C^3, 123.7; C^4, 137.9; C^5, 122.5; C^6, 153.7.

4.1.23. [Pd(η²-tmetc)(HN–SPh)]

The title complex was prepared in the same way as [Pd(η²-nq)(HN–SMe)] (yellow microcrystals, yield 88%). IR (in KBr) (cm^{-1}): $\nu_{C=O}$, 1736, 1699; $\nu_{C=N}$, 1601. ^{1}H-NMR (in $CDCl_3$, r.t.), δ (ppm): CH_2–S, 4.45 (2H, s); O–CH_3, 3.57 (6H, s), O–CH_3, 3.75 (6H, s); H^3, H^5, H^c, H^d, 7.31 (5H, m); H^b, H^4, 7.72 (3H, m); H^6, 9.21 (d, $J = 5.4$ Hz). $^{13}C\{^1H\}$-NMR (in $CDCl_3$, r.t.), δ (ppm): CH_2–S, 47.3; *C*=*C*, n.v.; O–CH_3, 52.2 (6C), O–CH_3, 52.3 (6C); ca. 132.7; C^b, 129.3; C^c, 132.5; C^d, 129.1; C^2, 157.3; C^3, 124.0; C^4, 138.0; C^5, 123.0; C^6, 153.9; *C*=O, 169.3, 169.6.

4.1.24. [Pd(η²-tmetc)(MeN–SPh)]

The title complex was prepared in the same way as [Pd(η²-nq)(HN–SMe)] (yellow microcrystals, yield 94%). IR (in KBr) (cm^{-1}): $\nu_{C=O}$, 1718, 1691 (d); $\nu_{C=N}$, 1603. ^{1}H-NMR (in $CDCl_3$, r.t.), δ (ppm): CH_2–S, 4.48 (2H, s); pyr–CH_3, 2.88 (3H, s); O–CH_3, 3.56 (6H, s); O–CH_3, 3.71 (6H, s); H^3, H^b, H^c, H^d, 7.26 (6H, m centr.); H^4, 7.57 (t, $J = 7.7$ Hz); H^5, 7.10 (d, $J = 7.4$ Hz). $^{13}C\{^1H\}$-NMR (in $CDCl_3$, r.t.), δ (ppm): CH_2–S, 46.9; pyr–CH_3, 28.5; *C*=*C* (obscured); O–CH_3, 52.1; C^b, 128.9; C^c, 129.3; C^d, 128.9; C^2, 161.9; C^3, 123.5; C^4, 137.9; C^5, 120.4; C^6, 157.0; *C*=O, 169.6.

4.1.25. [Pd(η²-tcne)(HN–SMe)]

The title complex was prepared in the same way as [Pd(η²-nq)(HN–SMe)] (yellow microcrystals, yield 89%). Found: C, 41.91; H, 2.33; N, 18.51. $C_{13}H_9N_5SPd$ requires: C, 41.78; H, 2.43; N, 18.74%. IR (in KBr) (cm^{-1}): $\nu_{C\equiv N}$, 2226 (s); $\nu_{C=N}$, 1599 (s). ^{1}H-NMR (in $CDCl_3$, r.t.), δ (ppm): CH_2–S, 4.3 (2H, s); S–CH_3, 2.58 (3H, s); H^3, 7.63 (d, $J = 7.7$ Hz); H^4, 8.01 (td, $J = 7.7$, 1.6 Hz); H^5, 7.54 (dd, $J = 7.7$, 5.4 Hz); H^6, 8.87 (d, $J = 5.4$ Hz). $^{13}C\{^1H\}$-NMR (in $(CD_3)_2CO$, r.t.), δ (ppm): CH_2–S, 44.7; S–CH_3; 20.6; *C*≡N, 114.7; C^2, 161.0; C^3, 126.3; C^4, 141.4; C^5, 126.2; C^6, 154.1.

4.1.26. [Pd(η²-tcne)(HN–SEt)]

The title complex was prepared in the same way as [Pd(η²-nq)(HN–SMe)] (yellow microcrystals, yield 98%). IR (in KBr) (cm^{-1}): $\nu_{C\equiv N}$, 2224 (s); $\nu_{C=N}$, 1603. ^{1}H-NMR (in $CDCl_3$, r.t.), δ (ppm): CH_2–S, 4.31 (2H, bs); S–CH_2, 2.95 (2H, q, $J = 7.4$ Hz); CH_2–CH_3, 1.50 (3H, t, $J = 7.4$ Hz); H^3, 7.63 (d, $J = 7.7$ Hz); H^4, 8.02 (t, $J = 7.7$ Hz,); H^5, 7.55 (dd, $J = 7.7$, 5.1 Hz); H^6, 8.86 (d, $J = 5.1$ Hz). $^{13}C\{^1H\}$-NMR (in $CDCl_3$, r.t.), (ppm): CH_2–S, 41.7; S–CH_2, 31.4; CH_2–CH_3, 14.0; *C*≡N, 113.2; C^2, 158.33; C^3, 125.1; C^4, 139.8; C^5, 124.1; C^6, 153.

4.1.27. [Pd(η²-tcne)(HN–S^{i}Pr)]

The title complex was prepared in the same way as [Pd(η²-nq)(HN–SMe)] (yellow microcrystals, yield 88%). IR (in KBr) (cm^{-1}): $\nu_{C\equiv N}$, 2222 (s); $\nu_{C=N}$, 1605 (s). ^{1}H-NMR (in $CDCl_3$, r.t.), δ (ppm): CH_2–S, 4.32 (2H, s); S–CH, 3.30 (1H, sept, $J = 6.7$ Hz); CH(CH_3)$_2$, 1.51 (6H, d, $J = 6.7$ Hz); H^3, 7.63 (d, $J = 7.7$ Hz); H^4, 8.00 (td, $J = 7.7$, 1.5 Hz); H^5, 7.52 (dd, $J = 7.7$, 5.3 Hz); H^6, 8.82 (d, $J = 5.3$ Hz). $^{13}C\{^1H\}$-NMR (in $CDCl_3$, r.t.), δ (ppm): CH_2–S, 41.9; S–*C*H, 40.8; CH(CH_3)$_2$, 22.8; C_2, 158.7; C_3, 125.4; C_4, 140.2; C_5, 124.1; C_6, 153.

4.1.28. [Pd(η²-tcne)(HN–S^{t}Bu)]

The title complex was prepared in the same way as [Pd(η²-nq)(HN–SMe)] (yellow microcrystals, yield 87%). IR (in KBr) (cm^{-1}): $\nu_{C\equiv N}$, 2226 (s); $\nu_{C=N}$, 1602 (s). ^{1}H-NMR (in $CDCl_3$, r.t.), δ (ppm): CH_2–S, 4.33 (2H, s); C(CH_3)$_3$, 1.57 (9H, s); H^3, 7.65 (d, $J = 7.8$ Hz); H^4, 8.00 (td, $J = 7.8$ Hz, 1.6 Hz); H^5, 7.31 (dd, $J = 7.8$, 5.3 Hz); H^6, 8.82 (d, $J = 5.3$ Hz). $^{13}C\{^1H\}$-NMR (in $CDCl_3$, r.t.), δ (ppm): CH_2–S, 38.8; S–*C*, 50.7; C(CH_3)$_3$, 30.1; *C*≡N, 113.1; C^2, 158.9; C^3, 125.1; C^4, 139.9; C^5, 123.6; C^6, 152.7.

4.1.29. [Pd(η²-tcne)(HN–SPh)]

The title complex was prepared in the same way as [Pd(η²-nq)(HN–SMe)] (yellow microcrystals, yield 83%). IR (in KBr) (cm^{-1}): $\nu_{C\equiv N}$, 2224 (s); $\nu_{C=N}$, 1603 (s). ^{1}H-NMR (in $CDCl_3$, r.t.), δ (ppm): CH_2–S, 4.63 (2H, s); H^4, 7.99 (td, $J = 7.7$, 7.1 Hz); H^3, H^5, H^b, H^c, H^d, 7.58 (7H, m); H^6, 8.89 (d, $J = 5.2$ Hz). $^{13}C\{^1H\}$-NMR (in $(CD_3)_2CO$, r.t.), δ (ppm): CH_2–S, 46.59; *C*≡N, 114.4; C^b, 131.8; C^c, 131.0; C^d, 130.8; C^2, 160.2; C^3, 126.4; C^4, 141.5; C^5, 125.8; C^6, 153.8.

4.1.30. [Pd(η²-tcne)(MeN–SPh)]

The title complex was prepared in the same way as [Pd(η²-nq)(HN–SMe)] (yellow microcrystals, yield 88%). IR (in KBr) (cm^{-1}): $\nu_{C\equiv N}$, 2232 (s); $\nu_{C=N}$, 1605. ^{1}H-NMR (in $CDCl_3$, r.t.), δ (ppm): CH_2–S, 4.67 (2H, s); pyr–CH_3 (3H, s); H^4, 7.83 (t, $J = 7.7$ Hz); H^5, 7.36 (d, $J = 7.7$ Hz); H^3, H^b, H^d, 7.53 (6H, m). $^{13}C\{^1H\}$-NMR (in $CDCl_3$, r.t.), δ (ppm): CH_2–S, 46.8; pyr–CH_3, 29.7; C^b, 130.6; C^c, 131.0; C^d, 130.4; C^2, 161.8; C^3, 125.0; C^4, 139.9; C^5, 121.0; C^6, 157.3.

5. IR and NMR measurements

The IR, ^{1}H-, and $^{13}C\{^1H\}$-NMR spectra were recorded on a Nicolet Magna™ 750 spectrophotometer and on a Bruker AC™ 200 spectrometer, respectively. The temperature-dependent ^{1}H-NMR spectra were ana-

Table 5
Crystallographic data for complexes [Pd(η^2-ma)(HN–S^{t}Bu)] and [Pd(η^2-tcne)(HN–SMe)

Empirical formula	$C_{14}H_{17}NO_3PdS$	$C_{13}H_9N_5PdS$
Formula weight	385.75	373.71
Crystal system	Triclinic	Monoclinic
Space group	$P\bar{1}$ (No. 2)	$P2_1/c$
Unit cell dimensions		
a (Å)	9.016(4)	10.21(1)
b (Å)	9.126(4)	9.517(8)
c (Å)	9.903(4)	14.95(1)
α (°)	112.18(3)	90
β (°)	96.03(3)	100.62(8)
γ (°)	102.32(3)	90
Volume (Å^3)	721.5(5)	1431(2)
Z	2	4
D_{calc} (Mg m^{-3})	1.776	1.735
Crystal color, habit	Yellow, block	Yellow, block
Crystal size (mm)	$0.15\times0.12\times0.07$	$0.15\times0.12\times0.11$
Diffractometer	Nicolet Siemens R3n/V	Nicolet Siemens R3n/V
Wavelength (Å)	0.71073	0.71073
μ (Mo–K$_\alpha$) (cm^{-1})	14.39	14.39
Temperature (K)	293(2)	293(2)
Θ Range for data collection (°)	2.3–25	2.5–22.1
Number of reflections collected	2556	1864
Number of unique reflections	2338 [$R_{int}=0.0249$]	1753 [$R_{int}=0.050$]
Absorption correlation	Empirical, ψ-scan	Empirical, ψ-scan
T_{max}/T_{min}	0.968/0.686	1.00/0.683
Refinement method	Full-matrix least-squares on F^2	Full-matrix least-squares on F^2
Number of data/parameters	2556/182	1699/182
Goodness-of-fit	1.077	1.155
$R(F)$ [a] [$I>2\sigma(I)$]	0.024	0.063
$R(wF^2)$ [a]	0.055	0.164
Largest diff. peak and hole (e Å^{-3})	0.361 and −0.412	1.09 and −1.13

[a] $R(F)=\Sigma(||F_o|-|F_c||)/\Sigma|F_o|$; $R(wF^2)=[\Sigma[w(F_o^2-F_c^2)^2]/\Sigma[w(F_o^2)^2]]^{1/2}$.

lyzed using the SWAN program [26] and the first-order rate constants determined were fitted to the appropriate temperatures by a reparametrized Eyring–Polanyi equation [27].

6. Kinetic and equilibrium measurements

The kinetics of olefin substitution were studied by addition of known aliquots of tmetc solutions to solutions of the complex under study in $CHCl_3$ ($[Pd]_0 \approx 10^{-4}$ mol dm^{-3}) in the thermostatted cell compartment of a Lambda 40 Perkin–Elmer spectrophotometer at the designed temperature. The reactions were followed by recording spectral changes in the wavelength range of 300–540 nm or at a suitable fixed wavelength.

Equilibrium studies were performed by addition of microaliquots of a solution of the designed olefin (or ligand) to a solution of the complex under study at a controlled temperature (25°C). The spectral features of the resulting mixtures were recorded by means of a Lambda 40 Perkin–Elmer spectrophotometer. Mathematical and statistical data analysis was carried out on a personal computer equipped with a locally adapted version of Marquardt's algorithm [28] written in TURBOBASIC™.

7. X-ray structural analysis

Data collection, crystal, and refinement parameters are collected in Table 5. Accurate values for the unit-cell dimensions were determined from the angular setting of 50 reflections with Θ between 9 and 14° and intensity data were measured using the ω–2Θ scan technique. The structures were solved using heavy-atom methods, completed by subsequent difference Fourier synthesis, and refined on F^2 by full-matrix least-squares procedures. All non-hydrogen atoms were refined with anisotropic displacement coefficients and all assigned hydrogen atoms were treated as idealized contributions. All software and sources of the scattering factors are contained in the SHELXTL/PC (version 5.03) program library [29].

8. Supplementary material

Tables of atomic coordinates and isotropic thermal parameters, bond lengths and angles, anisotropic thermal parameters, and H-atom coordinates are available upon request. Crystallographic data for the structural analysis have been deposited with the Cambridge Crystallographic Data Centre for compound **X**. Copies of this information may be obtained free of charge from: The Director, CCDC, 12 Union Road, Cambridge, CB2 1EZ, UK (Fax: +44-1223-336033; e-mail: deposit@ccdc.cam.ac.uk or www: http://www.ccdc.cam.ac.uk).

References

[1] (a) B. Crociani, F. Di Bianca, P. Uguagliati, L. Canovese, A. Berton, J. Chem. Soc. Dalton Trans. (1991) 71. (b) B. Crociani, S. Antonaroli, F. Di Bianca, L. Canovese, F. Visentin, P. Uguagliati, J. Chem. Soc. Dalton Trans. (1994) 1145. (c) L. Canovese, F. Visentin, P. Uguagliati, F. Di Bianca, S. Antonaroli, B. Crociani, J. Chem. Soc. Dalton Trans. (1994) 3113. (d) L. Canovese, F. Visentin, P. Uguagliati, B. Crociani, F. Di Bianca, Inorg. Chim. Acta 45 (1995) 235. (e) B. Crociani, S. Antonaroli, M. Paci, F. Di Bianca, L. Canovese, Organometallics 16 (1997) 384. (f) L. Canovese, F. Visentin, P. Uguagliati, G. Chessa, V. Lucchini, G. Bandoli, Inorg. Chim. Acta 275 (1998) 385. (g) L. Canovese, F. Visentin, P. Uguagliati, G. Chessa, A. Pesce, J. Organomet. Chem. 566 (1998) 61. (h) B. Crociani, S. Antonaroli,

G. Bandoli, L. Canovese, F. Visentin, P. Uguagliati, Organometallics 18 (1999) 1137. (i) L. Canovese, F. Visentin, G. Chessa, A. Niero, P. Uguagliati, Inorg. Chim. Acta 293 (1999) 44.
[2] L. Canovese, F. Visentin, P Uguagliati, F. Di Bianca, A. Fontana, B. Crociani, J. Organomet. Chem. 508 (1996) 101.
[3] L. Canovese, F. Visentin, P. Uguagliati, B. Crociani, J. Chem. Soc. Dalton Trans. (1996) 1921.
[4] R. Van Asselt, C.J. Elsevier, W.J.J. Smeets, A.L. Speck, Inorg. Chem. 33 (1994) 1521.
[5] P.T. Cheng, C.D. Cook, S.C. Nyburg, K.Y. Wan, Inorg. Chem. 10 (1971) 2210.
[6] F. Ozawa, T. Ito, Y. Nakamura, A. Yamamoto, J. Organomet. Chem. 168 (1979) 375.
[7] C.D. Cook, K.Y. Wan, Inorg. Chem. 10 (1971) 2696.
[8] R. Van Asselt, C.J. Elsevier, Tetrahedron 50 (1994) 323.
[9] F. Gomez-de la Torre, F.A. Jalon, A. Lopez-Agenjo, B.R. Manzano, A. Rodriguez, T. Sturm, W. Weissensteiner, M. Martinez-Ripoll, Organometallics 17 (1998) 4634 and references therein.
[10] M. Tschoerner, G. Trabesinger, A. Albinati, P.S. Pregosin, Organometallics 16 (1997) 3447.
[11] (a)R. Van Asselt, C.J. Elsevier, J. Mol. Catal. 65 (1991) L13. (b) R. Van Asselt, C.J. Elsevier, Organometallics 11 (1992) 1999.(c) B.M. Trost, D.L. van Vranken, Chem. Rev. 96 (1996) 395.
[12] A. Tsubouchi, N. Nakamura, A. Sugimoto, H. Inoue, T. Adachi, J. Heterocyclic Chem. 31 (1994) 1327.
[13] F.H. Allen, S. Bellard, M.D. Brice, B.A. Cartwright, A. Doubleday, H. Higgs, T. Hummlink, B.G. Hummlink-Peters, O. Kennard, W.D.S. Motherwell, J.R. Rodgers, D.G. Watson, Acta Crystallogr. Sect. B 35 (1979) 2331.
[14] G. Huttner, I. Jibril, Angew. Chem. Int. Ed. Engl. 23 (1984) 740.
[15] C.G. Pierjont, R.M. Buchanan, H.H. Downs, J. Organomet. Chem. 124 (1977) 103.
[16] M. Kranenburg, J.G.P. Delis, P.C.J. Kramer, P.W.N.M. van Leeuwen, K. Vrieze, N. Veldman, A.L. Spek, K. Goubitz, J. Fraanje, J. Chem. Soc. Dalton Trans. (1997) 1839
[17] R.G. Little, D. Pantler, P. Coppens, Acta Crystallogr. Sect. B 27 (1971) 1493.
[18] (a) E.W. Abel, D.G. Evans, J.R. Koe, V. Sik, M.B. Hursthouse, P.A. Bates, J. Chem. Soc. Dalton Trans. (1989) 2315. (b) E.W. Abel, J.C. Dormer, K.G. Ellis, V. Sik, M.B. Hursthouse, M.A. Mazid, J. Chem. Soc. Dalton Trans. (1992) 107.
[19] L. Canovese, in press.
[20] K. Selvakumar, M. Valentini, M. Worle, P.S. Pregosin, A. Albinati, Organometallics 18 (1999) 1207.
[21] H.D. Beckhaus, Angew. Chem. Int. Ed. Engl. 17 (1978) 593.
[22] P. Uguagliati, A. Benedetti, S. Enzo, L. Schiffini, Comput. Chem. 8 (1984) 161.
[23] J.K. Kochi, Organometallic Mechanisms and Catalysis, Academic Press, New York, 1978 (Chapter 17) and references therein.
[24] T. Ukai, H. Kawazura, Y. Ishii, J.J. Bonnet, J.A. Ibers, J. Organomet. Chem. 65 (1974) 253.
[25] W.L.F. Armarego, D.D. Perrin, Purification of Laboratory Chemicals, third ed., Pergamon, New York, 1988.
[26] G. Balacco, J. Chem. Inf. Comput. Sci. 34 (1994) 1235.
[27] P. Uguagliati, R.A. Michelin, U. Belluco, R. Ros, J. Organomet. Chem. 169 (1979) 115.
[28] D.W. Marquardt, SIAM J. Appl. Math. 11 (1963) 431.
[29] G. Sheldrick, SHELXTL/PC (version 5.03), Siemens XRD, Madison WI.